Prediction of Multiple Hydrogen Ligation at a Vanadium(II) Site in a Metal-Organic Framework

Romit Chakraborty,[†,‡] Kurtis M. Carsch,[†,‡] David E. Jaramillo,[†,‡] Yuto Yabuuchi,[†,‡] Hiroyasu Furukawa,[†,‡] Jeffrey R. Long,[†,¶,§,‡] and Martin Head-Gordon [*,¶,‡,‡]

†*Materials Sciences Division, Lawrence Berkeley National Laboratory, Berkeley California*
‡*Department of Chemistry, University of California, Berkeley*
¶*Chemical Sciences Division, Lawrence Berkeley National Laboratory, Berkeley California*
§*Department of Chemical and Biomedical Engineering, University of California, Berkeley*

E-mail: romit@berkeley.edu,mhg@cchem.berkeley.edu

Abstract

Densifying hydrogen in a metal-organic framework (MOF) at moderate pressures can circumvent challenges associated with high pressure compression. The highly tunable structural and chemical composition in MOFs affords vast possibilities to optimize binding interactions. At the heart of this search are the nanoscale characteristics of molecular adsorption at the binding site(s). Using density functional theory (DFT) to model binding interactions of hydrogen to the exposed metal site of cation-exchanged MFU-4l, we predict multiple hydrogen ligation of H_2 at the first coordination sphere of V(II) in V(II)-exchanged MFU-4l. We find that the strength of this binding between the metal site and H_2 molecules can be tuned by altering the halide counterion adjacent to the metal site and that the fluoride containing node affords the most favourable

interactions for high density H_2 storage. Using energy decomposition analysis, we delineate electronic contributions that enable multiple hydrogen ligation and demonstrate its benefits for hydrogen adsorption and release at modest pressures.

A major challenge for a future hydrogen-based economy is the need for energy intensive compression and liquefaction of H_2 to counteract its low volumetric energy density.[1,2] Current machinery for hydrogen distribution for vehicular storage involves compression above 350 bar,[3] where the majority of the operating cost at the refuelling station is due to the compressor.[4] In addition to environmental and energy costs of such high-pressure treatment, storage of a highly compressed flammable gas is a safety concern for vehicle operators. Metal-organic frameworks (MOFs) offer a potential solution to this problem as a broad class of new materials that can, if appropriately designed, adsorb and release H_2 at more moderate pressures.[5]

As a materials design problem, optimization of MOFs for hydrogen storage is an enormous challenge, with a complex interplay between constraints imposed by the desired functional characteristics, and non-trivial synthetic considerations. The high surface to volume ratio in a MOF combined with its structural and chemical tunability result in combinatorial numbers of possibilities for the design of an optimal storage material.[5,6] Nonetheless, the syntheses and measurements of new MOF combinations are time-consuming and resource-intensive, prompting the need for computationally aided approaches. Reliable quantum chemical calculations can screen candidate materials to identify promising leads, at a minimum. Design principles for high-density hydrogen storage can also be derived from computational prediction of the electronic structure of hydrogen interacting with the MOF binding site and the associated pore.[7] In-silico characterizations of the feature space in MOFs can identify the leading contributors to interactions and thereby offer a pathway to release H_2 below operating pressures of 100 bar.

In the list of technical targets for vehicular storage, the US Department of Energy (DOE) has earmarked volumetric storage capacity at 40 g/L by the year 2025 at operating condi-

tions in the range of $[-40, 60]\,°C$ and 5 to 12 bar.[8] The current record for physisorptive storage is held by Ni$_2$-m-dobdc (dobdc=1,4-dioxido-1,3-benzenedicarboxylate) with a volumetric capacity of 11 g/L at $25\,°C$ for a pressure swing between 100 and 5 bar.[9] Evidently, physisorption-driven storage alone does not suffice for room temperature storage applications, and stronger binding interactions are desirable.[5,6,10,11] Given the demand for high density storage of hydrogen in the solid state,[12,13] it is highly desirable to bind *multiple* hydrogens at an open metal site in a MOF with binding enthalpies in the 15-25 kJ/mol range though this has not yet been demonstrated. Indeed there have been very few demonstrations of multiple H$_2$ binding at any potentially realistic site.[14–17]

Strong H$_2$-binding to a five-coordinate V(II) center in V$_2$Cl$_{2.8}$(btdd), which displays an isosteric heat of 21 kJ/mol,[18] provides promise for ambient temperature storage of hydrogen. Guided by this insight, we wanted to explore analogous H$_2$ binding to V(II) in a four-coordinate scaffold with two available coordination sites, which could potentially be accessed within MFU-4*l*. Toward this objective, we predict feasible ligation of two hydrogen molecules to V(II) in V(II) exchanged MFU-4*l* which has been previously prepared and characterized in a hydrated form.[19] Furthermore the parent material, MFU-4*l* has the benefit of being able to readily tune the peripheral anion, which can modulate the binding energetics of H$_2$.

The parent MFU-4l framework is highly robust and demonstrates exceptional thermal stability.[20,21] The defining feature of MFU-4*l* is scorpionate-type coordination with BTDD^{2-} ligands ((H$_2$BTDD = bis(1H-1,2,3-triazolo[4,5-*b*],[4',5'-])dibenzo[1,4]dioxin))) at these tetrahedral metal sites, where a tridentate ligand speared with nitrogens binds the metal in a *fac* manner. The term scorpionate [22] derives from two donor sites grasping at the metal like the pincers of a scorpion followed by a third and final donor, the stinger, reaching over the plane formed by the metal site and the two donors. The peripheral Zn(II) ions in MFU-4*l* can be exchanged for a variety of transition metal divalent cations.[19,23–26] This material piqued our interest for two reasons: i) it features 4 outer metal sites per node that have tetrahedral coordination, and ii) metal-exchange for V(II), which is known to favour octahe-
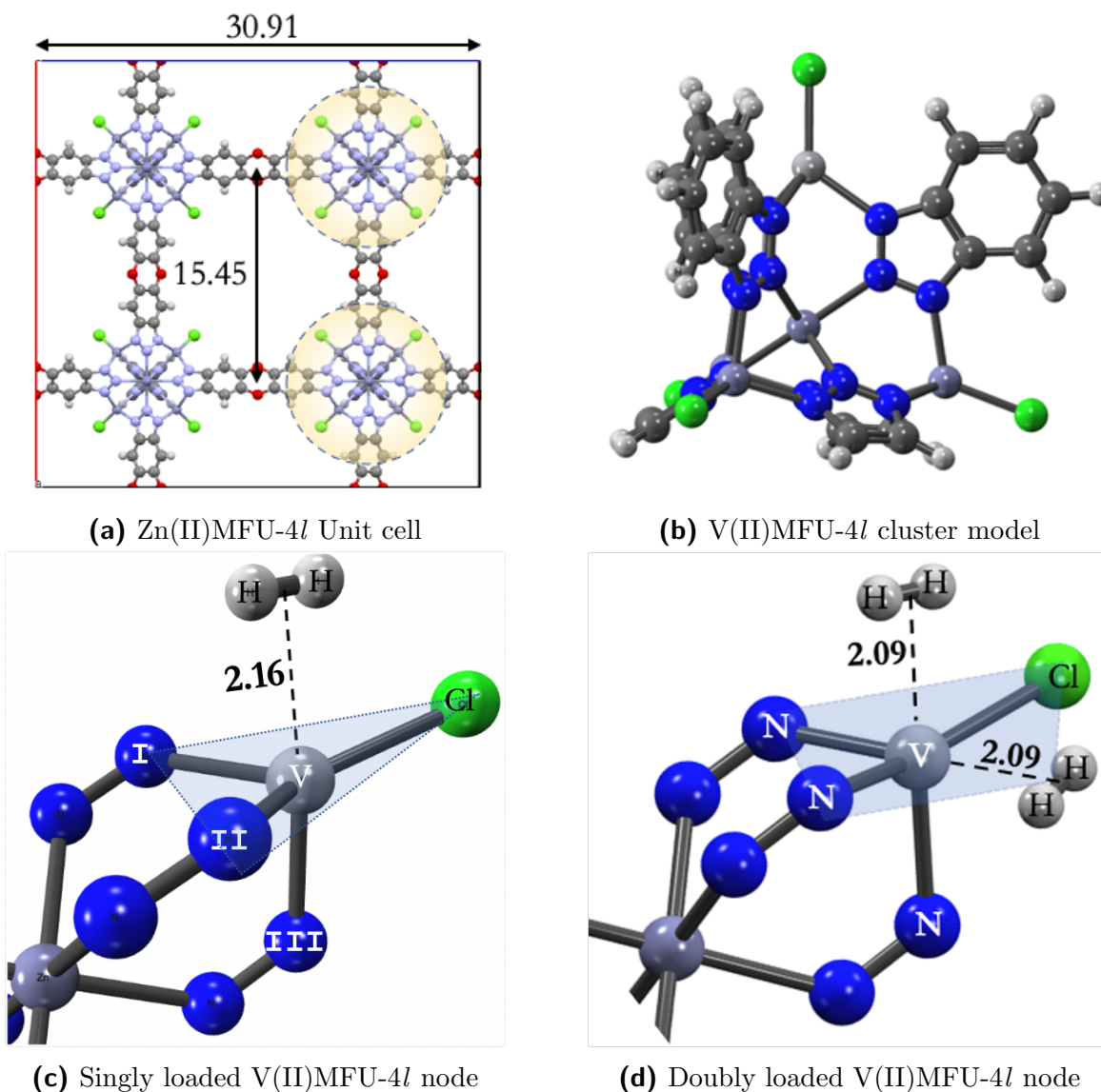
(a) Zn(II)MFU-4*l* Unit cell

(b) V(II)MFU-4*l* cluster model

(c) Singly loaded V(II)MFU-4*l* node

(d) Doubly loaded V(II)MFU-4*l* node

Figure 1: a) Cubic cell unit of Zn(II)MFU-4*l*, the parent material for the transmetallated V(II)MFU-4*l* studied here. b) Cluster model for V(II)MFU-4*l* with Cl⁻ ions. Figures c) and d) are closeup views of the equilibrium geometries of singly and doubly loaded V(II)MFU-4*l*. Vanadium sites are rendered in grey, nitrogen in blue, chloride in green and Zn in violet grey. Distances are labeled in Å.

dral coordination, has been reported[19] for these sites. Figure 1a shows the cubic unit cell of Zn(II)MFU-4*l*. Here we consider each node to behave independently. The pentanuclear cluster model shown in Fig. 1b was built from the parent scaffold. Binding environment around the V(II) site was modeled by truncation of the node at its benzotriazolate extremities and a triazolate truncation of the linker was employed elsewhere giving a molecular formula of

V(II)$_1$Zn(II)$_4$Cl$_4$(btz)$_3$(tz)$_3$ (btz = benzotriazolate, tz = triazolate) to the cluster. An octahedral Zn(II) at the center of the node is surrounded by 4 peripheral tetrahedral sites, one of which is substituted with V(II). Following experimental characterization of H$_2$ binding to V(II) in a similar ligand-field environment in V$_2$Cl$_{2.8}$(btdd)[18] we model V(II) in its high-spin (S=3/2) ground state.

The MOF crystal is periodic and three dimensional, and upon approach of a guest molecule to a metal site, there may be strong binding contributions reflecting local chemical interactions at the site, supplemented by weaker long-range dispersion interactions. To ensure accurate description of the critical local chemistry, we employ the ωB97M-V functional,[27] which is an accurate range-separated hybrid metaGGA that includes non-local VV10 dispersion,[28] designed by the combinatorial "survival of the most transferable" protocol. ωB97M-V was the top-performing hybrid density functional in several large assessments, including the MGC84 database,[29] the large and diverse GMTKN55 benchmark dataset,[30–32] and the TMC151 transition metal database.[33] These findings are buttressed by a recent extensive benchmark[34,35] of density functionals for hydrogen storage. Employing ωB97M-V limits calculations to a cluster node, as exact exchange is not feasible for periodic calculations. We have chosen our cluster model to be very faithful to the full MOF for capturing metal-ligand interactions at short distances, and adequate for capturing the leading contributions from comparatively long-range dispersion forces that prevail in MOF pores. Geometries were optimized in the def2-SVP basis that contains f-polarization at the transition metal site, and p polarization at the hydrogens. The def2-ECP effective core potential was used for elements heavier than Rb (Z=37) such as iodine.[36] Single point calculations were performed with this basis augmented with the fairly large Karlsruhe def2-TZVPPD basis[37,38] in the binding region with 2f and 1g polarization functions at the metal site and 3p and 1d polarization functions for hydrogen. Geometries were converged to 3×10^{-4} kJ/mol in energy, and 3×10^{-5} a.u in the maximum gradient component. Counterpoise corrections proposed by Boys and Bernardi[39] were employed to reduce basis set superposition error (BSSE) in
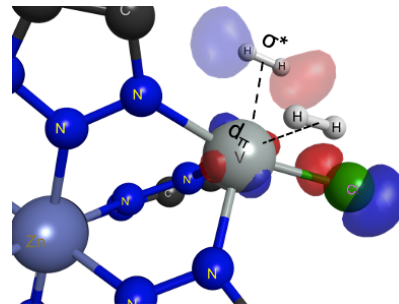
energy evaluations.

Figures 1c. and 1d. show close-ups of equilibrium geometries for single and double-hydrogen loaded V(II)MFU-4l nodes, with Cl$^-$. The second hydrogen binds closer to the metal site with a center of mass distance of 2.09 Å (the first H$_2$ binds at 2.16 Å). The singly loaded node assumes a distorted trigonal bipyramidal configuration around the V(II) site (see Fig. 1c) with the equatorial plane formed by the chloride ion and nitrogens I and II, and the axial sites occupied by hydrogen and nitrogen III. The axial H$_2$ and N$_{III}$ make angles of 90.6° and 91.31° with the equatorial N$_{II}$. The doubly loaded node forms a distorted octahedron around the V(II) site with the bonding axes of two hydrogens aligned nearly perpendicular to one-another. Completion of the octahedron at the metal site brings both hydrogens inward in the coordination sphere which is indicative of stronger binding interactions. In going from zero to one, to two hydrogens bound, the V(II)-Cl distance changes from 2.30, to 2.33, to 2.39 Å.

To decompose metal-H$_2$ binding into physically meaningful interactions, we use Energy Decomposition Analysis (EDA), a tool based on Absolutely Localized Molecular Orbitals (ALMOs).[40–42] Here the MOF node and its ligated hydrogen(s) are partitioned into two interacting fragments. Separate single-point calculations were performed on them followed by a block diagonal reassembly of MO coefficients to give the frozen density matrix and energy (Δ Frz). Polarization is described using a basis of fragment electric-field response functions (FERFs) which allows a fragment orbital to adjust to the weak electric field of its counterpart resulting in dipolar and quadrupolar responses.[43] Finally, the charge transfer term Δ CT is computed from the difference between the completely relaxed and polarized electron density. Preparation energy (Δ Prep) is the energy required to distort the unbound MOF node and free hydrogen into their bound configuration. Δ E is the sum of all electronic contributions to binding and Δ H evaluated at 77 K includes the effect of vibrations of nuclear modes at finite temperature. Columns I and II in Table 2a list energy contributions Δ for single (V(II)-H$_2$) and double (V(II)H$_2$-H$_2$) loading, and Column III shows changes

E(kJ/mol)	$V(II)L_3Cl$-H_2	$V(II)L_3ClH_2$-H_2	$\Delta\Delta$
Δ Prep	8.8	11.1	2.3
Δ Frz	19.8	18.3	**-1.5**
Δ Pol	-11.9	-13.9	**-2.0**
Δ CT	-30.0	-32.8	**-2.8**
Δ $H_2 \rightarrow V(II)$	-23.4	-26.1	**-2.7**
Δ $V(II) \rightarrow H_2$	-6.6	-6.7	**-0.1**
Δ E	-13.3	-17.3	**-4.0**

(a)

(b)

Figure 2: a) Comparison of Energy Decomposition of the first and second H_2 binding to V(II)(Cl)MFU-4*l*. Cooperative binding of H_2 to V(II) in MFU-4*l* is predicted by increase in binding energy on adsorption of the second hydrogen. b) Complimentary Occupied-Virtual pair (COVP) of charge transfer orbitals for backdonation from V(II) to the second ligated H_2.

$(\Delta\Delta = \Delta_2 - \Delta_1)$ in each term for sequential ligation of the two hydrogens. Both hydrogens bind with charge transfer terms greater than 30 kJ/mol. Charge transfer was stronger for the second H_2 with a $\Delta\Delta$ of -2.8 kJ/mol, along with a 2.0 kJ/mol increase in polarization interactions. Stronger short-range interactions on binding of the second H_2 is consistent with completion of the octahedral coordination sphere around vanadium(II) and counteracts the reorganization energy ($\Delta\Delta$ Prep) required to bind the second H_2. Not only do we find two hydrogens bound strongly at the metal site, but the second equilvalent of H_2 binds 4.0 kJ/mol more strongly than binding for the first H_2. A negative $\Delta\Delta E$ that is largely driven by short-range interactions (charge transfer and polarization) shows that rearrangement at the binding site promotes ligation of the second hydrogen due to favorable orbital overlap; or in other words the electronic binding energy of 2 hydrogens exhibits positive cooperativity.

The d^3 configuration in distorted square-pyramidal V(II) has been known to favour interactions with π acids for two reasons. First, the empty d_{z^2} orbital avoids potential antibonding σ^* interactions and enables close ligand approach. Second, a half filled d_π manifold is able to engage in backbonding where the effective range is shorter than that of the σ bond.[44,45] The pentacoordinate V(II) in MFU-4*l* is distorted trigonal bipyramidal (TBP) and transitions to a distorted octahedron on loading of the second hydrogen. To explore this further

we used a perturbative approach[40] to separate forward from back-donation. Donation from the hydrogen σ orbital to the empty metal d_{z^2} is the dominant charge transfer contributor offering -23.4 and -26.1 kJ/mol of stabilization for the first and second hydrogen loading. At shorter distances, favorable π overlap is afforded by the metal d_π backdonation to hydrogen σ^* resulting in sizeable contributions of -6.6 and 6.7 kJ/mol for binding the first and the second H_2. Strikingly, the presence of the first bound H_2 causes forward donation from the second H_2 to be strengthened with the back-donation remaining nearly identical.

Complementary Occupied-Virtual Pairs (COVPs) constructed from unitary transformations within the occupied and virtual subspaces of the two fragments (the MOF node and hydrogen) provide a physical picture for orbitals engaged in forward- and back-bonding. While the set of all COVPs exactly describes charge transfer between the fragments, the major energetic (and charge) contributions to bonding arises from one or two significant COVPs.[40] Charge transfer orbitals for V(II) to H_2 backbonding in Fig. 2b plotted with an isodensity contour of 0.06 shows d_π orbitals of V(II) engaging with the hydrogen σ^* orbital. A closer inspection of the back-donating orbital at the MOF node reveals contribution from the p_z orbital on the chloride ligand bound to V(II) (see Fig. 2b). This motivated an investigation of the effect of halide substitution on the binding strength of hydrogen with the MOF node. Table 1 lists the binding energies for the sequential loading of two hydrogens onto the V(II)MFU-4l node represented as a V(II)L$_3$X complex containing an X$^-$ halide bound to the metal. Among different halides, an F$^-$ was found to promote the most favorable H_2 binding energies. Heavier halide ligands, especially in the case of Br$^-$, show strong comparative stabilization on binding the second H_2. This effect is driven by a stronger charge transfer term dominated by forward donation from H_2 to V(II). Thus, the halide ligand can be used to finely tune the strength of multiple H_2 binding with V(II) in this material.

Energy lowering upon H_2 binding is countered by the entropic tendency of the bound hydrogen to gain translational and rotational freedom. The free energy change on binding describes the balance between these two terms and determines the adsorption isotherm. We

estimate the enthalpy and Gibbs free energy change of binding muliple hydrogens to the node with a standard frequency analysis at the B3LYP-D2/def2-SVP/RRHO level of theory and employ anharmonic 1D corrections to zero point vibrational energies (ZPVEs) for the frustrated modes of H_2. Low frequency (≤ 100 cm^{-1}) normal modes were raised to 100 cm^{-1} for evaluation of the enthalpic and entropic terms to correct for the well-known breakdown of the harmonic oscillator model for soft vibrations.[46] The binding of each hydrogen adds 5 modes to the system due to the frustrated translations and rotation of bound H_2 on the MOF surface. Anharmonic 1D corrections to the ZPVEs of these modes were computed by employing the Fourier Grid Hamiltonian[47] to solve for the vibrational spectrum by sampling with 1D PES with finite displacements scans around the equilibrium binding configuration with the framework held rigid. Details pertaining to anharmomic corrections to the ZPVE are included in Section I of the SI. A scaling factor of $s = 0.9893$ obtained from quartic force fields was added to the B3LYP-D2 ZPVEs to account for anharmonic coupling between vibrational modes.[48]

Table 2 lists changes in binding energy, enthalpy, and free energies for the sequential binding of two hydrogens to V(II)MFU-4l at the temperature of liquid nitrogen (77 K) and 1 atm pressure. Thermal excitation of soft framework modes (< 100 cm^{-1}) are dampened at such low temperatures and the entropic penalty of binding is small compared to the

Table 1: Binding energy and its decomposition for ligation of two hydrogens to the V(II)MFU-4l node represented as V(II)L$_3$X cluster model with L standing for the chelating nitrogens of the scorpionate SBU and X$^-$ as the placeholder for the halide counterion. All contributions are in kJ/mol.

Fragments	X$^-$	ΔPrep	ΔFrz+Disp	ΔPol	ΔCT	ΔForw	ΔBack	ΔE
V(II)L$_3$X-H$_2$	F$^-$	6.7	8.6	-10.0	-28.4	-22.6	-5.8	-23.1
	Cl$^-$	8.8	19.8	-11.9	-30.1	-23.4	-6.6	-13.3
	Br$^-$	10.5	19.3	-11.9	-28.0	-22.5	-5.5	-10.1
	I$^-$	8.9	25.2	-13.9	-31.6	-25.6	-6.0	-11.5
V(II)L$_3$XH$_2$-H$_2$	F$^-$	9.1	12.2	-11.4	-29.2	-23.0	-6.2	-19.3
	Cl$^-$	11.1	18.3	-13.9	-32.8	-26.1	-6.7	-17.3
	Br$^-$	11.8	20.9	-15.5	-34.3	-28.0	-6.3	-17.1
	I$^-$	14.9	22.8	-17.2	-35.7	-29.4	-6.3	-15.3

Table 2: Binding Energy, Enthalpy, and Free Energy at 77 K and 1 atm for H_2 binding to V(II)XMFU-4l, X = F$^-$, Cl$^-$, Br$^-$, I$^-$. $\Delta\Delta$ values correspond to changes on second hydrogen loading ($\Delta_2 - \Delta_1$). All values are in kJ/mol.

X$^-$	ΔE_1	ΔE_2	$\Delta\Delta E$	$\Delta H_1(T)$	$\Delta H_2(T)$	$\Delta\Delta H(T)$	$T\Delta S_1(T)$	$T\Delta S_2(T)$	$\Delta G_1(T)$	$\Delta G_2(T)$	$\Delta\Delta G(T)$
F$^-$	-23.1	-19.3	3.8	-19.3	-14.5	4.8	-7.1	-6.9	-12.2	-7.6	4.6
Cl$^-$	-13.3	-17.3	**-4.0**	-9.0	-10.3	**-1.3**	-7.0	-7.1	-2.0	-3.2	**-1.2**
Br$^-$	-10.1	-17.1	**-7.0**	-6.7	-9.3	**-2.6**	-7.0	-7.3	0.3	-2.0	**-2.3**
I$^-$	-11.5	-15.4	**-3.9**	-5.8	-7.6	**-1.8**	-7.1	-7.2	1.3	-0.5	**-1.8**

enthalpy of binding. We employ a stoichiometric two-site model suggested by Dill and Bromberg [49] to predict binding isotherms. Hydrogen binds the V(II) center in the sequence $\langle \mathrm{V} + \mathrm{H}_2 \xrightarrow{K_1} \mathrm{V}-\mathrm{H}_2 + \mathrm{H}_2 \xrightarrow{K_2} \mathrm{V}-2\,\mathrm{H}_2 \rangle$. The binding curve, determined by the average number of gas molecules $v = \langle i \rangle$ bound as a function of partial pressure p at temperature T, is given by

$$v(p,T) = \frac{d\ln(Q)}{d\ln(p)}, \quad \text{where} \quad Q = 1 + K_1(T)p + K_1(T)K_2(T)p^2 \tag{1}$$

which is the binding polynomial that sums over the ligation states V, V$-$H$_2$ and V$-2\,$H$_2$. Equilibrium constants $K_i(T)$ were determined by the free energy of adsorption $\Delta G_i^\circ(T)$ at the standard pressure of 1 atm (1.01325 bar). Dimensionless surface coverage (θ) can be converted into measures for usable capacity by making use of crystallographic information. The MFU-4l unit cell is cubic with each edge L measuring 30.91 Å. A unit cell contains 8 nodes (n_N), each bearing 4 tetrahedral sites (n_o) that are capable of binding a maximum of two hydrogens (n_{H_2}). Assuming all tetrahedral sites in the node are transmetallated with V(II), the amount of hydrogen adsorbed with each site doubly occupied is given by $\frac{n_N \times n_o \times n_{\mathrm{H}_2} \times m_{\mathrm{H}_2}}{L^3} = 7.25$ g/L. The smaller unit cell dimension ($L = 21.63$ Å) in MFU-4,[50] which contains the same type of nodes studied here, results in denser packing of metal sites and an increased maximum allowed hydrogen uptake of 21.18 g/L.[1] The secondary axis of binding curves in Fig. 3 shows predictions of total hydrogen uptake in g/L in V(II)MFU-4l. Since these predictions correspond to H$_2$ bound at the V sites and do not account for

---

[1]These estimates assume negligible changes in unit cell dimensions upon metal exchange of the parent Zn(II) material

additional H_2 that will physisorb within the pore, they are estimates of the lower bounds for uptake. Advanced Grand Canonical Monte Carlo (GCMC) models for surface coverage such as the ones formulated by Snurr and coworkers[10,51] can be used predict surface coverage due to dispersion interactions of H_2 with the pore that also takes into account other structural parameters of the MOF such as surface area and free volume.

Strong uptake is seen at liquid nitrogen temperature at low pressures (0-1 bar) with almost all sites saturated by 0.5 bar for the F^- and Cl^- ligated node. The isotherm for the Br^- containing nodes shows sigmoidal shape with comparatively slower uptake in the low pressure regime. The strongly negative $\Delta\Delta E$ for the Br^- containing node is attenuated when one considers the effect of ZPVEs and vibrational contributions to the enthalpy of and free energy binding. Consequently, the binding isotherm at 77 K does not show a clear step on the ligation of the second H_2 (see fig. 3a). Weak binding in V(II)(I)MFU-4l results in a small percentage of sites being occupied. Open metal sites in MOFs that saturate after binding one H_2 would give overwhelmingly positive $\Delta\Delta H$ and $\Delta\Delta G$. Only the fluoride containing node shows a small positive $\Delta\Delta H(T) = 4.8$ kJ/mol ($\Delta\Delta G = 4.6$ kJ/mol). This node accomodates two hydrogens with strong binding enthalpies of $\Delta H_1(T) = -19.3$ and $\Delta H_2(T) = -14.5$ kJ/mol at liquid nitrogen temperatures. Consequently, the binding curves show a very steep uptake in the low pressure (0-0.1 bar) range at 77 K.

Cooling to cryogenic temperatures (-90°C/183 K or lower) is expensive and for practical applications of a nanoporous material one would want steep uptake at cool temperatures that are relatively inexpensive to access. Hence we look at the binding curve at -45°C (228 K) in Fig. 3b. The corresponding energy, enthalpy and free energy changes are reported in

Table 3: Binding Energy, Enthalpy, and Free Energy at 228 K (-45 °C) and 1 atm for H_2 binding to V(II)XMFU-4l, X = F^-, Cl^-, Br^-, I^-.

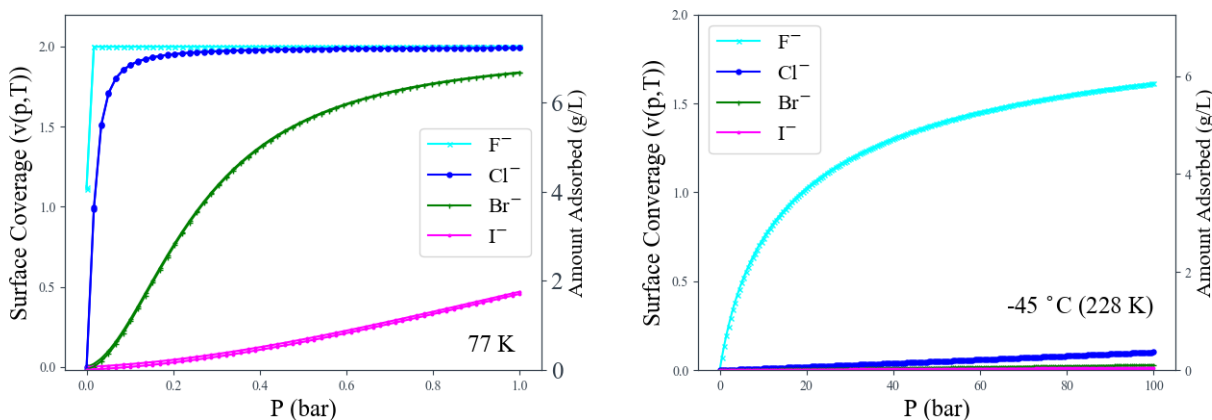| X^-	ΔE_1	ΔE_2	$\Delta\Delta E$	$\Delta H_1(T)$	$\Delta H_2(T)$	$\Delta\Delta H(T)$	$T\Delta S_1(T)$	$T\Delta S_2(T)$	$\Delta G_1(T)$	$\Delta G_2(T)$	$\Delta\Delta G(T)$
F^-	-23.1	-19.3	3.8	-21.3	-16.3	5.0	-24.9	-23.9	3.6	7.5	4.0
Cl^-	-13.3	-17.3	**-4.0**	-10.6	-13.3	**-2.7**	-23.8	-26.4	13.2	13.1	**-0.1**
Br^-	-10.1	-17.1	**-7.0**	-8.4	-12.8	**-4.4**	-23.9	-27.7	15.6	14.8	**-0.7**
I^-	-11.5	-15.4	**-3.9**	-7.7	-11.6	**-4.0**	-24.7	-28.1	17.0	16.5	**-0.5**

Figure 3: Predicted binding curve for halide variants of V(II)MFU-4*l* at the temperature of liquid nitrogen (a) and at 228 K (-45 °C) (b).

Table. 3. V(II)(F)MFU-4*l* emerges with the steepest uptake for the 100-5 bar pressure swing. We estimate the usable capacity of the F^- containing V(II)MFU-4*l* node at 4.1 g/L at 228 K. For the MFU-4 scaffold, which has a higher density of metal sites whilst retaining the same nodes, we predict a usable capacity of 11.9 g/L under these conditions. Interestingly, the predicted entropic penalty for binding the second hydrogen is greater when compared to that for the first for V(II)MFU-4*l* nodes containing heavier halides (Cl^-, Br^-, and I^-) which offsets the stronger electronic binding energy for ligation of the second H_2.

A key element in the materials design challenge for high volumetric density hydrogen storage in MOFs is the ability to reversibly bind multiple hydrogens at the first coordination sphere of a metal site. We predict that the V(II)MFU-4*l* node containing fluoride ligands can bind two hydrogen molecules per metal with binding enthalpies in the range of 15-25 kJ/mol. When compared to conventional open site metals in MOFs (e.g Cu(I)MFU-4*l*),

Table 4: Usable Capacity at 228 K (-45 °C) for the fluoride containing node in MFU-4*l* and MFU-4.

	Amount Adsorbed (g/L)	
P (bar)	MFU-4*l*	MFU-4
5	1.8	5.2
100	5.8	17.1
Usable Capacity (g/L)	4.1	11.9

12

two H_2s binding to V(II) in V(II) exchanged MFU-4*l* doubles the volumetric capacity of the material at liquid nitrogen temperatures, and offers strong uptake in the 100-5 bar pressure swing at -45°C.

Consistent with the completion of octahedral coordination at the V(II) site, binding of the second hydrogen in the presence of the first is accompanied by an increase in charge transfer between the metal and hydrogen. Forward donation from H_2 to V(II) increases with the ligation of the second hydrogen to the node with back-donation from the metal site remaining largely unchanged. Nodes containing heavier halides, especially Br^-, show stronger binding for ligation of the second hydrogen at the V(II), but this energy lowering is counteracted by a commensurate increase in the entropic penalty. Change in binding behaviour with different halide ions in the node suggests that the anion coordinated to the binding site in this material can be used to finely tune the binding strength with H_2 or other guests. The MFU-4*l* parent scaffold, which has been shown to allow a broad range of metal substitutions at its tetrahedral metal sites, is critical in accommodating two hydrogens at the V(II) site. Provided the synthetic challenge of realizing a stable material with suitable density of V(II) sites is met, this strategy can be used to enable high density H_2 storage at close to ambient temperatures of -45°C. Thus, V(II)-MFU-4*l* and V(II)-MFU-4 represent promising candidate materials for the coordination of multiple H_2 molecules.

Acknowledgement

Supporting Information Available

Coordinates for all converged geometries, and further details pertaining to all computations and experiments performed are included in the supplementary material. All electronic structure computations reported in this work were performed with the standard version of the Q-Chem 5.4 software package.[52]

References

(1) Crabtree, G. W.; Dresselhaus, M. S.; Buchanan, M. V. The hydrogen economy. *Physics today* **2004**, *57*, 39–44.

(2) Armstrong, R. C.; Wolfram, C.; De Jong, K. P.; Gross, R.; Lewis, N. S.; Boardman, B.; Ragauskas, A. J.; Ehrhardt-Martinez, K.; Crabtree, G.; Ramana, M. The frontiers of energy. *Nature Energy* **2016**, *1*, 1–8.

(3) Sdanghi, G.; Maranzana, G.; Celzard, A.; Fierro, V. Review of the current technologies and performances of hydrogen compression for stationary and automotive applications. *Renewable and Sustainable Energy Reviews* **2019**, *102*, 150–170.

(4) Reddi, K.; Elgowainy, A.; Rustagi, N.; Gupta, E. Impact of hydrogen refueling configurations and market parameters on the refueling cost of hydrogen. *International Journal of Hydrogen Energy* **2017**, *42*, 21855–21865.

(5) Murray, L. J.; Dincă, M.; Long, J. R. Hydrogen storage in metal–organic frameworks. *Chemical Society Reviews* **2009**, *38*, 1294–1314.

(6) Suh, M. P.; Park, H. J.; Prasad, T. K.; Lim, D.-W. Hydrogen storage in metal–organic frameworks. *Chemical reviews* **2012**, *112*, 782–835.

(7) Allendorf, M. D.; Hulvey, Z.; Gennett, T.; Ahmed, A.; Autrey, T.; Camp, J.; Cho, E. S.; Furukawa, H.; Haranczyk, M.; Head-Gordon, M., et al. An assessment of strategies for

the development of solid-state adsorbents for vehicular hydrogen storage. *Energy & Environmental Science* **2018**, *11*, 2784–2812.

(8) DOE Technical Targets for Onboard Hydrogen Storage for Light-Duty Vehicles, Department of Energy. `https://www.energy.gov/eere/fuelcells/doe-technical-targets-onboard-hydrogen-storage-light-duty-vehicles`.

(9) Kapelewski, M. T.; Runčevski, T.; Tarver, J. D.; Jiang, H. Z.; Hurst, K. E.; Parilla, P. A.; Ayala, A.; Gennett, T.; Fitzgerald, S. A.; Brown, C. M.; Long, J. R. Record High Hydrogen Storage Capacity in the Metal-Organic Framework Ni_2(m-dobdc) at Near-Ambient Temperatures. *Chemistry of Materials* **2018**, *30*, 8179–8189.

(10) Bae, Y. S.; Snurr, R. Q. Optimal isosteric heat of adsorption for hydrogen storage and delivery using metal–organic frameworks. *Microporous and Mesoporous Materials* **2010**, *132*, 300–303.

(11) Bueno-Pérez, R.; García-Pérez, E.; Gutiérrez-Sevillano, J. J.; Merkling, P. J.; Calero, S. A Simulation Study of Hydrogen in Metal–Organic Frameworks. **2010**, *28*, 823–835.

(12) Schneemann, A.; Wan, L. F.; Lipton, A. S.; Liu, Y. S.; Snider, J. L.; Baker, A. A.; Sugar, J. D.; Spataru, C. D.; Guo, J.; Autrey, T. S.; Jørgensen, M.; Jensen, T. R.; Wood, B. C.; Allendorf, M. D.; Stavila, V. Nanoconfinement of Molecular Magnesium Borohydride Captured in a Bipyridine-Functionalized Metal-Organic Framework. *ACS Nano* **2020**, *14*, 10294–10304.

(13) Schneemann, A.; White, J. L.; Kang, S.; Jeong, S.; Wan, L. F.; Cho, E. S.; Heo, T. W.; Prendergast, D.; Urban, J. J.; Wood, B. C.; Allendorf, M. D.; Stavila, V. Nanostructured Metal Hydrides for Hydrogen Storage. *Chemical Reviews* **2018**, *118*, 10775–10839.

(14) Tsivion, E.; Veccham, S. P.; Head-Gordon, M. High-Temperature Hydrogen Storage of Multiple Molecules: Theoretical Insights from Metalated Catechols. *ChemPhysChem* **2017**, *18*, 184–188.

(15) Sagara, T.; Klassen, J.; Ortony, J.; Ganz, E. Binding energies of hydrogen molecules to isoreticular metal-organic framework materials. *The Journal of Chemical Physics* **2005**, *123*, 014701.

(16) Runčevski, T.; Kapelewski, M. T.; Torres-Gavosto, R. M.; Tarver, J. D.; Brown, C. M.; Long, J. R. Adsorption of two gas molecules at a single metal site in a metal–organic framework. *Chemical Communications* **2016**, *52*, 8251–8254.

(17) Tachikawa, H.; Iyama, T. Mechanism of hydrogen storage in the graphene nanoflake-lithium-H2 system. *Journal of Physical Chemistry C* **2019**, *123*, 8709–8716.

(18) Jaramillo, D. E.; Jiang, H. Z.; Evans, H. A.; Chakraborty, R.; Furukawa, H.; Brown, C. M.; Head-Gordon, M.; Long, J. R. Ambient-Temperature Hydrogen Storage via Vanadium (II)-Dihydrogen Complexation in a Metal–Organic Framework. *Journal of the American Chemical Society* **2021**, *143*, 6248–6256.

(19) Comito, R. J.; Wu, Z.; Zhang, G.; Lawrence, J. A.; Korzyński, M. D.; Kehl, J. A.; Miller, J. T.; Dincă, M. Stabilized Vanadium Catalyst for Olefin Polymerization by Site Isolation in a Metal–Organic Framework. *Angewandte Chemie - International Edition* **2018**, *57*, 8135–8139.

(20) Biswas, S.; Grzywa, M.; Nayek, H. P.; Dehnen, S.; Senkovska, I.; Kaskel, S.; Volkmer, D. A cubic coordination framework constructed from benzobistriazolate ligands and zinc ions having selective gas sorption properties. *Dalton transactions* **2009**, 6487–6495.

(21) Schmieder, P.; Denysenko, D.; Grzywa, M.; Baumgärtner, B.; Senkovska, I.; Kaskel, S.; Sastre, G.; van Wüllen, L.; Volkmer, D. CFA-1: the first chiral metal–organic framework containing Kuratowski-type secondary building units. *Dalton Transactions* **2013**, *42*, 10786–10797.

(22) Trofimenko, S. Recent advances in poly(pyrazolyl)borate (scorpionate) chemistry. *Chem. Rev.* **1993**, *93*, 943–980.

(23) Dubey, R. J.; Comito, R. J.; Wu, Z.; Zhang, G.; Rieth, A. J.; Hendon, C. H.; Miller, J. T.; Dincă, M. Highly Stereoselective Heterogeneous Diene Polymerization by Co-MFU-4l: A Single-Site Catalyst Prepared by Cation Exchange. *Journal of the American Chemical Society* **2017**, *139*, 12664–12669.

(24) Denysenko, D.; Grzywa, M.; Jelic, J.; Reuter, K.; Volkmer, D. Scorpionate-Type Coordination in MFU-4l Metal–Organic Frameworks: Small-Molecule Binding and Activation upon the Thermally Activated Formation of Open Metal Sites. *Angewandte Chemie International Edition* **2014**, *53*, 5832–5836.

(25) Metzger, E. D.; Comito, R. J.; Hendon, C. H.; Dincă, M. Mechanism of single-site molecule-like catalytic ethylene dimerization in Ni-MFU-4l. *Journal of the American Chemical Society* **2017**, *139*, 757–762.

(26) Comito, R. J.; Metzger, E. D.; Wu, Z.; Zhang, G.; Hendon, C. H.; Miller, J. T.; Dincă, M. Selective Dimerization of Propylene with Ni-MFU-4l. *Organometallics* **2017**, *36*, 1681–1683.

(27) Mardirossian, N.; Head-Gordon, M. ωB97M-V: A combinatorially optimized, range-separated hybrid, meta-GGA density functional with VV10 nonlocal correlation. *The Journal of chemical physics* **2016**, *144*, 214110.

(28) Vydrov, O. A.; Van Voorhis, T. Nonlocal van der Waals density functional: The simpler the better. *Journal of Chemical Physics* **2010**, *133*, 244103.

(29) Mardirossian, N.; Head-Gordon, M. Thirty years of density functional theory in computational chemistry: an overview and extensive assessment of 200 density functionals. *Mol. Phys.* **2017**, *115*, 2315–2372.

(30) Goerigk, L.; Hansen, A.; Bauer, C.; Ehrlich, S.; Najibi, A.; Grimme, S. A look at the density functional theory zoo with the advanced GMTKN55 database for gen-

eral main group thermochemistry, kinetics and noncovalent interactions. *Phys. Chem. Chem. Phys.* **2017**, *19*, 32184–32215.

(31) Najibi, A.; Goerigk, L. The Nonlocal Kernel in van der Waals Density Functionals as an Additive Correction: An Extensive Analysis with Special Emphasis on the B97M-V and omega B97M-V Approaches. *J. Chem. Theory Comput.* **2018**, *14*, 5725–5738.

(32) Santra, G.; Martin, J. M. Some observations on the performance of the most recent exchange-correlation functionals for the large and chemically diverse GMTKN55 benchmark. **2019**, *2186*, 030004.

(33) Chan, B.; Gill, P. M. W.; Kimura, M. Assessment of DFT Methods for Transition Metals with the TMC151 Compilation of Data Sets and Comparison with Accuracies for Main-Group Chemistry. *J. Chem. Theory Comput.* **2019**, *15*, 3610–3622.

(34) Veccham, S. P.; Head-Gordon, M. Density Functionals for Hydrogen Storage: Defining the H2Bind195 Test Set with Ab Initio Benchmarks and Assessment of 55 Functionals. *J. Chem. Theory Comput.* **2020**, *16*, 4963–4982.

(35) Veccham, S. P.; Head-Gordon, M. Assessment of Performance of Density Functionals for Predicting Potential Energy Curves in Hydrogen Storage Applications. *The Journal of Physical Chemistry A* **2021**, *125*, 4245–4257.

(36) Sure, R.; Grimme, S. Corrected small basis set Hartree-Fock method for large systems. *Journal of computational chemistry* **2013**, *34*, 1672–1685.

(37) Weigend, F.; Ahlrichs, R. Balanced basis sets of split valence, triple zeta valence and quadruple zeta valence quality for H to Rn: Design and assessment of accuracy. *Physical Chemistry Chemical Physics* **2005**, *7*, 3297–3305.

(38) Rappoport, D.; Furche, F. Property-optimized Gaussian basis sets for molecular response calculations. *The Journal of chemical physics* **2010**, *133*, 134105.

(39) Boys, S. F.; Bernardi, F. The calculation of small molecular interactions by the differences of separate total energies. Some procedures with reduced errors. *Molecular Physics* **1970**, *19*, 553–566.

(40) Khaliullin, R. Z.; Cobar, E. A.; Lochan, R. C.; Bell, A. T.; Head-Gordon, M. Unravelling the origin of intermolecular interactions using absolutely localized molecular orbitals. *The Journal of Physical Chemistry A* **2007**, *111*, 8753–8765.

(41) Horn, P. R.; Mao, Y.; Head-Gordon, M. Probing non-covalent interactions with a second generation energy decomposition analysis using absolutely localized molecular orbitals. *Physical Chemistry Chemical Physics* **2016**, *18*, 23067–23079.

(42) Levine, D. S.; Head-Gordon, M. Energy decomposition analysis of single bonds within Kohn–Sham density functional theory. *Proceedings of the National Academy of Sciences of the United States of America* **2017**, *114*, 12649–12656.

(43) Horn, P. R.; Head-Gordon, M. Polarization contributions to intermolecular interactions revisited with fragment electric-field response functions. *Journal of Chemical Physics* **2015**, *143*.

(44) Lee, K. et al. Design of a metal-organic framework with enhanced back bonding for separation of N_2 and CH_4. *Journal of the American Chemical Society* **2014**, *136*, 698–704.

(45) Lee, K.; Howe, J. D.; Lin, L. C.; Smit, B.; Neaton, J. B. Small-molecule adsorption in open-site metal-organic frameworks: A systematic density functional theory study for rational design. *Chemistry of Materials* **2015**, *27*, 668–678.

(46) Ribeiro, R. F.; Marenich, A. V.; Cramer, C. J.; Truhlar, D. G. Use of solution-phase vibrational frequencies in continuum models for the free energy of solvation. *The Journal of Physical Chemistry B* **2011**, *115*, 14556–14562.

(47) Clay Marston, C.; Balint-Kurti, G. G. The Fourier grid Hamiltonian method for bound state eigenvalues and eigenfunctions. *The Journal of Chemical Physics* **1989**, *91*, 3571–3576.

(48) Kesharwani, M. K.; Brauer, B.; Martin, J. M. Frequency and zero-point vibrational energy scale factors for double-hybrid density functionals (and other selected methods): Can anharmonic force fields be avoided? *Journal of Physical Chemistry A* **2015**, *119*, 1701–1714.

(49) Dill, K. A.; Bromberg, S.; Stigter, D. *Molecular driving forces: statistical thermodynamics in biology, chemistry, physics, and nanoscience*; Garland Science, 2010; p 563.

(50) Denysenko, D.; Grzywa, M.; Tonigold, M.; Streppel, B.; Krkljus, I.; Hirscher, M.; Mugnaioli, E.; Kolb, U.; Hanss, J.; Volkmer, D. Elucidating gating effects for hydrogen sorption in MFU-4-type triazolate-based metal-organic frameworks featuring different pore sizes. *Chemistry - A European Journal* **2011**, *17*, 1837–1848.

(51) Frost, H.; Snurr, R. Q. Design requirements for metal-organic frameworks as hydrogen storage materials. *Journal of Physical Chemistry C* **2007**, *111*, 18794–18803.

(52) Epifanovsky, E.; Gilbert, A. T.; Feng, X.; Lee, J.; Mao, Y.; Mardirossian, N.; Pokhilko, P.; White, A. F.; Coons, M. P.; Dempwolff, A. L., et al. Software for the frontiers of quantum chemistry: An overview of developments in the Q-Chem 5 package. *The Journal of Chemical Physics* **2021**, *155*, 084801.

TOC Graphic